Supporting Information

New approaches to three-dimensional positive electrodes enabling scalable high areal capacity

Zhiyong Zhao[1], Xiaowei Zhang[1,], Peng Wang[1], Ioanna Maria Pateli[2], Hongyi Gao[3,4], Ge Wang[3,*], John T. S. Irvine[1,2,*]*

[1] Institute of Advanced Materials, Beijing Normal University, Beijing, 100875, China
[2] School of Chemistry, University of St Andrews, Fife KY16 9ST, St Andrews, UK
[3] Beijing Advanced Innovation Center for Materials Genome Engineering, Beijing Key Laboratory of Function Materials for Molecule & Structure Construction, School of Materials Science and Engineering, University of Science and Technology Beijing, Beijing, 100083, China
[4] Shunde Innovation School, University of Science and Technology Beijing, Shunde 528399, P. R. China

* Correspondence should be addressed to xiaoweizhang@bnu.edu.cn, gewang@ustb.edu.cn, and jtsi@st-andrews.ac.uk.

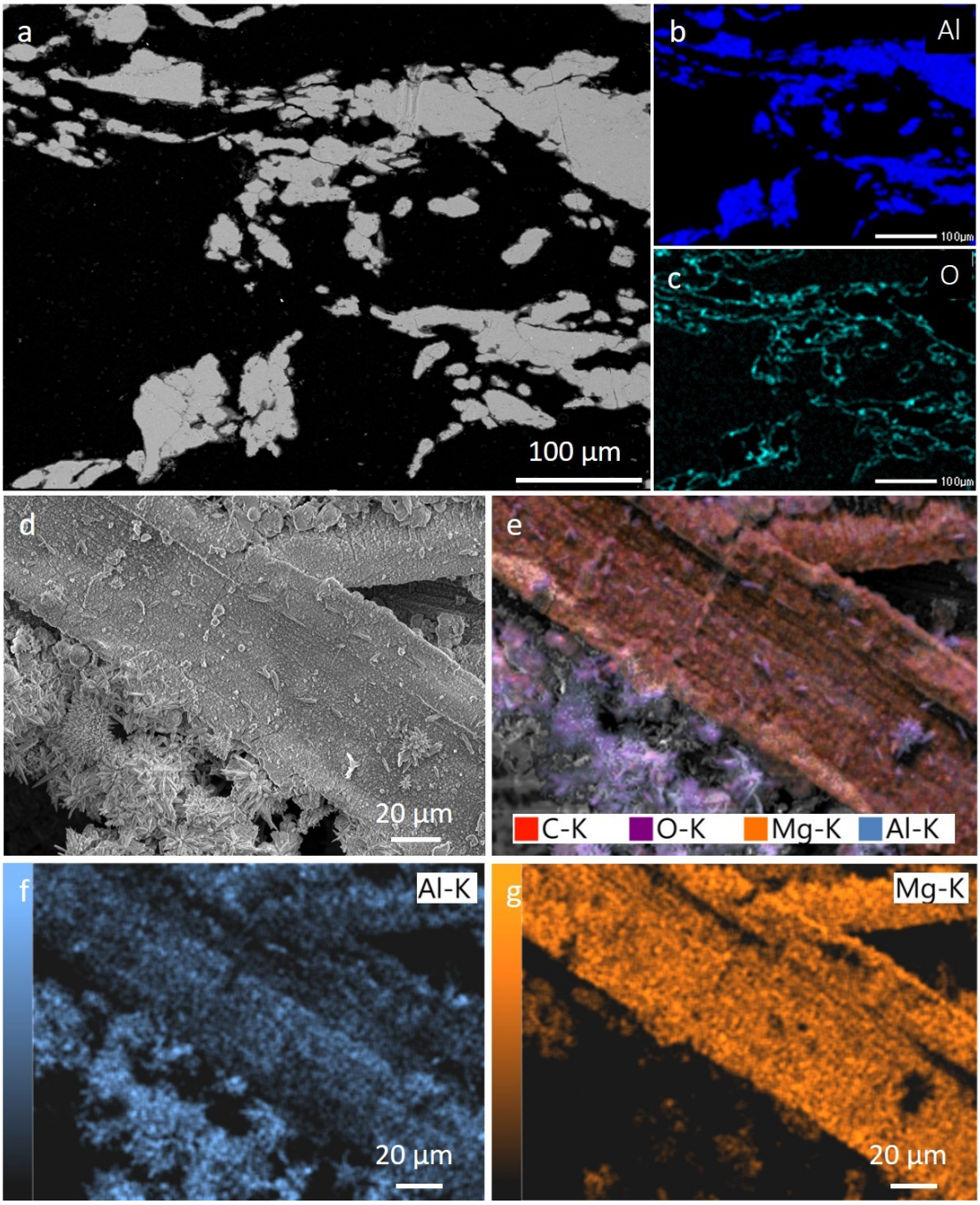

Figure S1. (a,d) Cross-section SEM image and (b,c,e,f,g) EDX elemental mapping images of the initial pAlN substrate before HCl treatment.

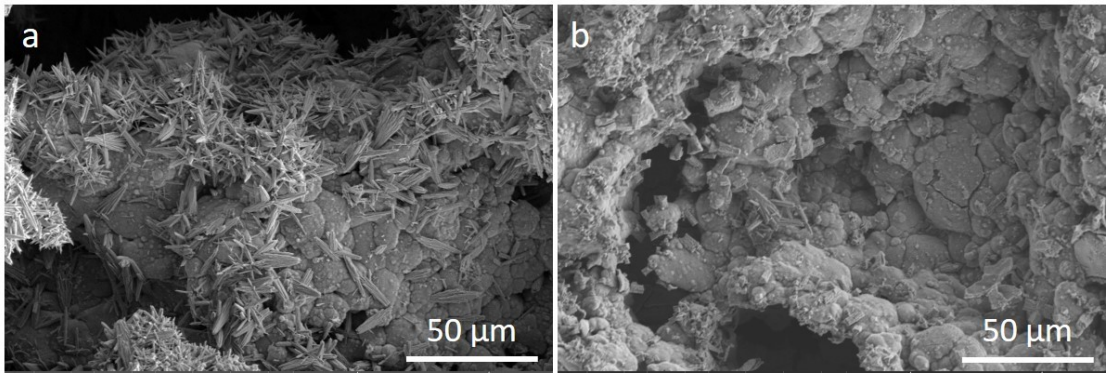

Figure S2. SEM images of the pAlN substrate (a) before and (b) after HCl treatment.

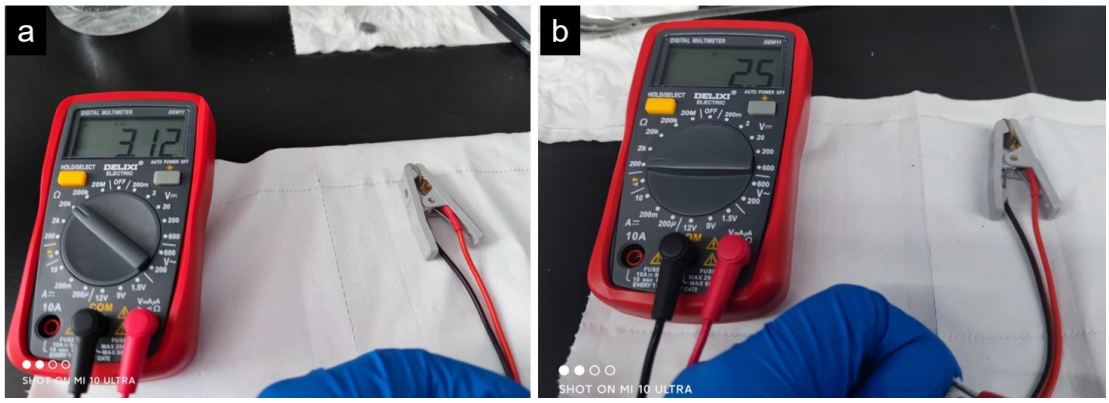

Figure S3. Resistance value of the pAlN substrate (a) before and (b) after HCl treatment.

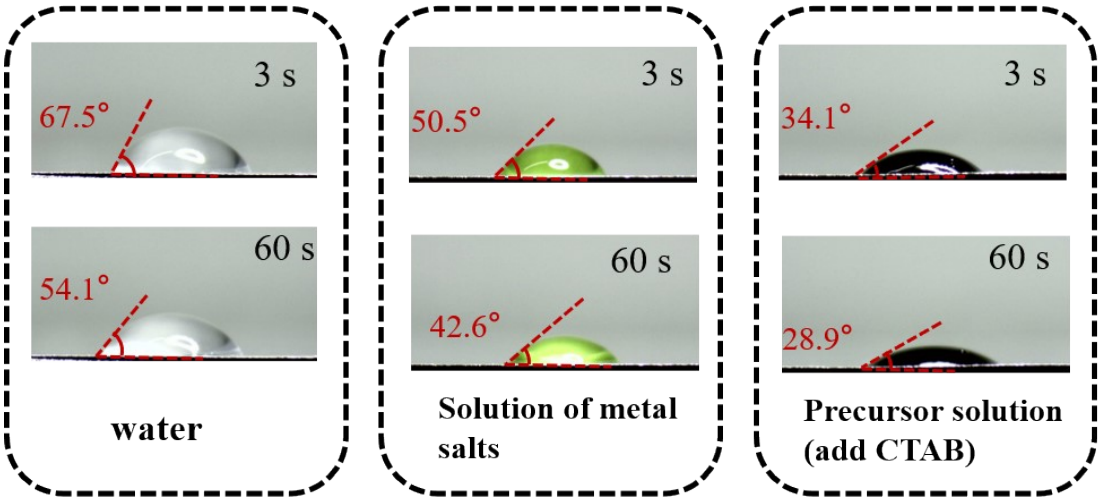

Figure S4. The wetting angles on Al foil using water, metal salt solution (mixture of $LiNO_3$, $Fe(NO_3)_3 \cdot 9H_2O$ and $NH_4H_2PO_4$) and precursor solution (mixture of $LiNO_3$, $Fe(NO_3)_3 \cdot 9H_2O$, $NH_4H_2PO_4$ and CTAB).

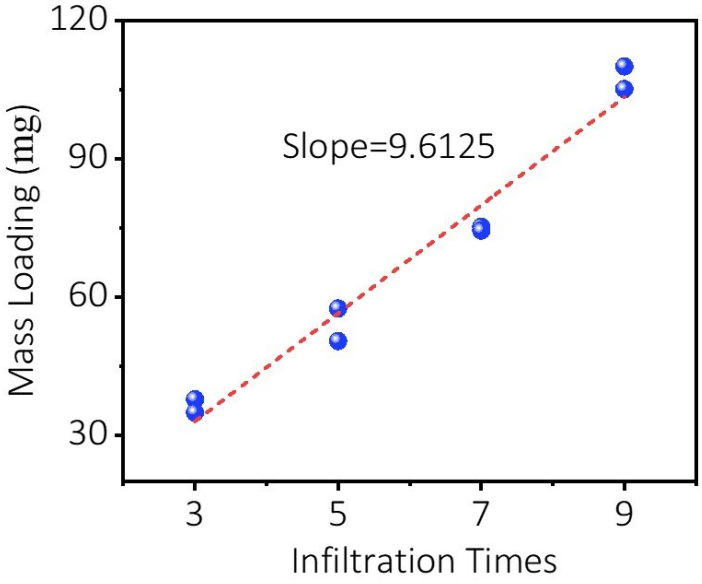

Figure S5. The relationship between the mass loading and the infiltration times.

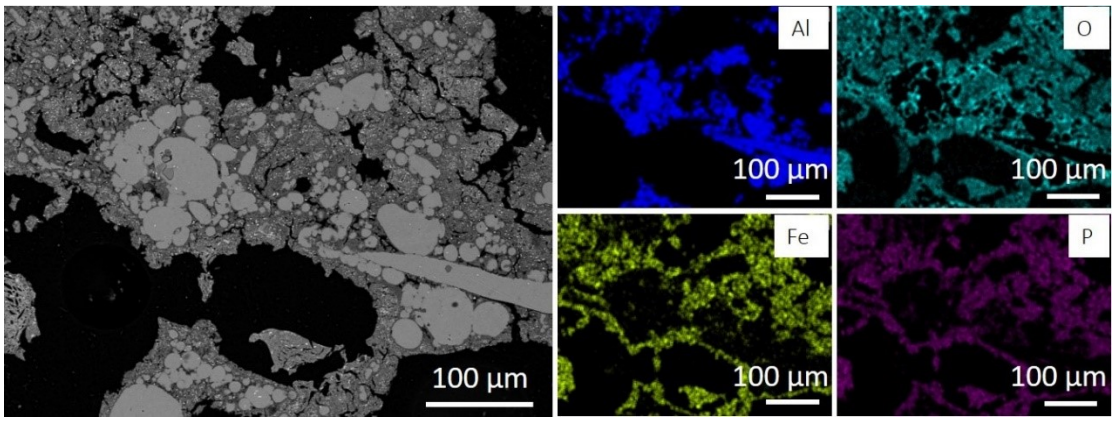

Figure S6. SEM image and EDX elemental mapping of the polished cross-section of the 3D LFP/pAlN electrode.

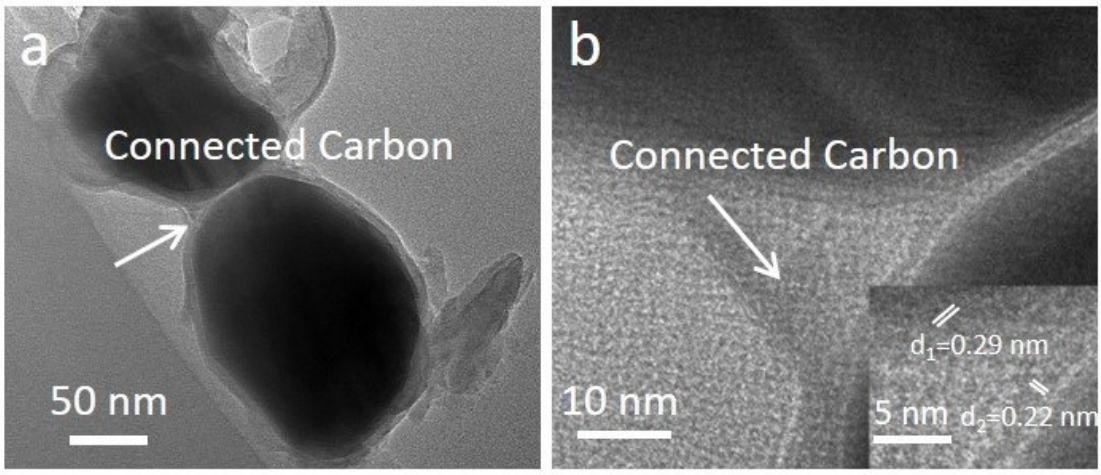

Figure S7. (a) TEM image and (b) HRTEM image of the nanoparticles ground from the 3D LFP/pAlN electrode.

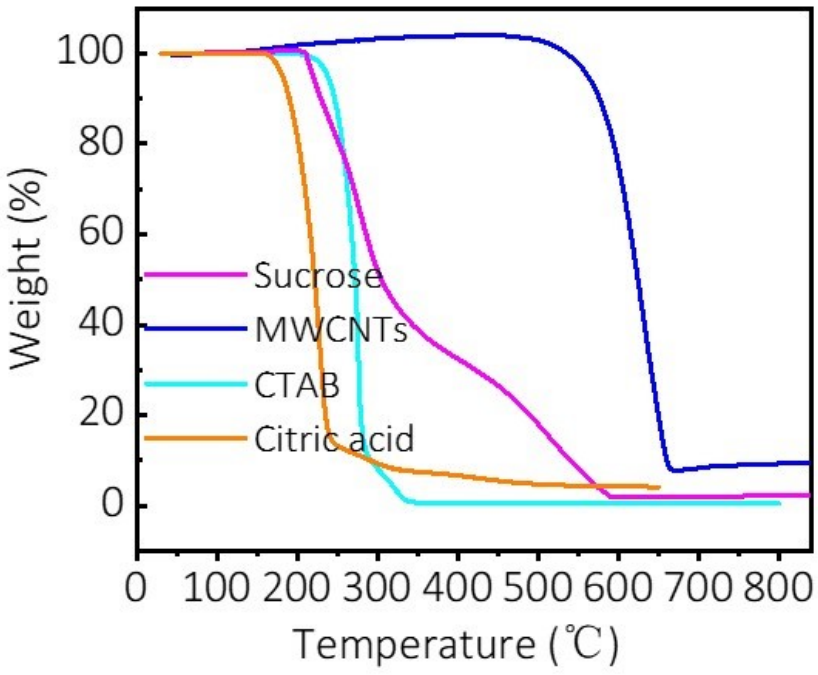

Figure S8. TGA curves of sucrose, MWCNTs, CTAB and citric acid measured under air atmosphere.

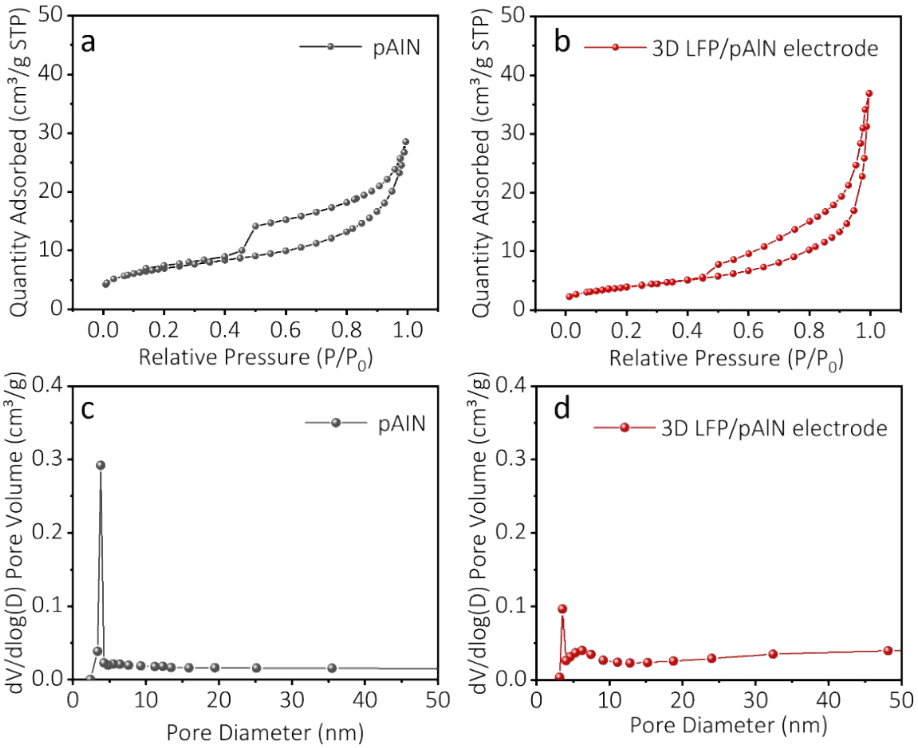

Figure S9. N_2 adsorption isotherms of (a) pAIN and (b) 3D LFP/pAIN electrode. Pore size distribution curves of (c) pAIN and (d) 3D LFP/pAIN electrode.

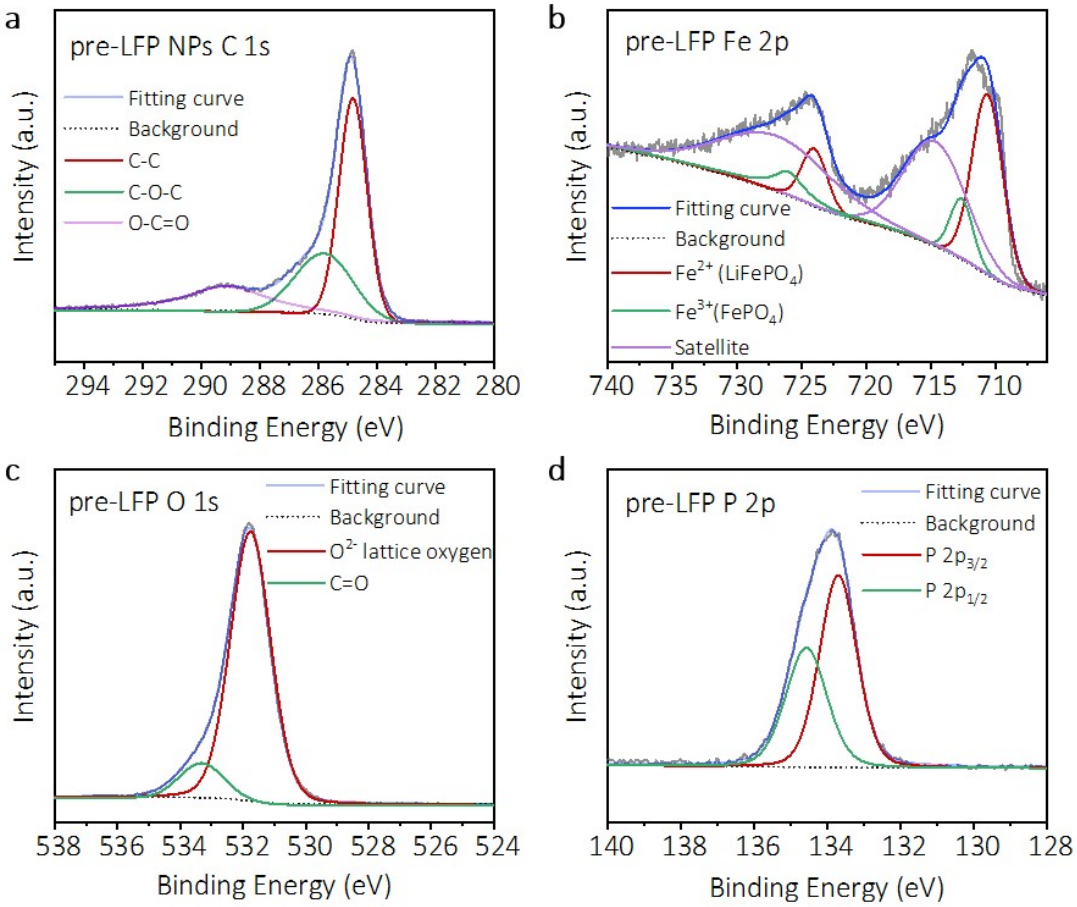

Figure S10. High-resolution XPS spectra of (a) C 1s, (b) Fe 2p, (c) O 1s and (d) P 2p for commercial carbon-coating pre-LFP NPs.

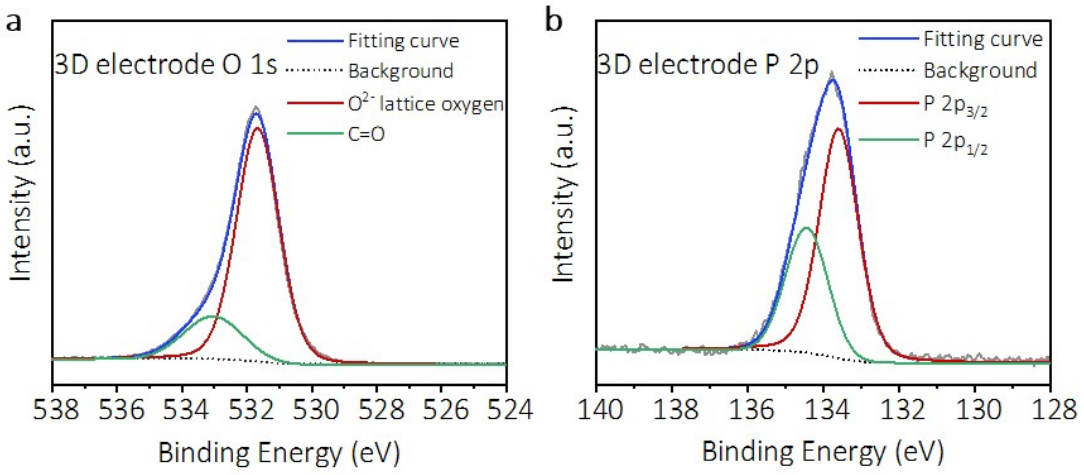

Figure S11. High-resolution XPS spectra of (a) O 1s and (b) P 2p for 3D LFP/pAlN electrode.

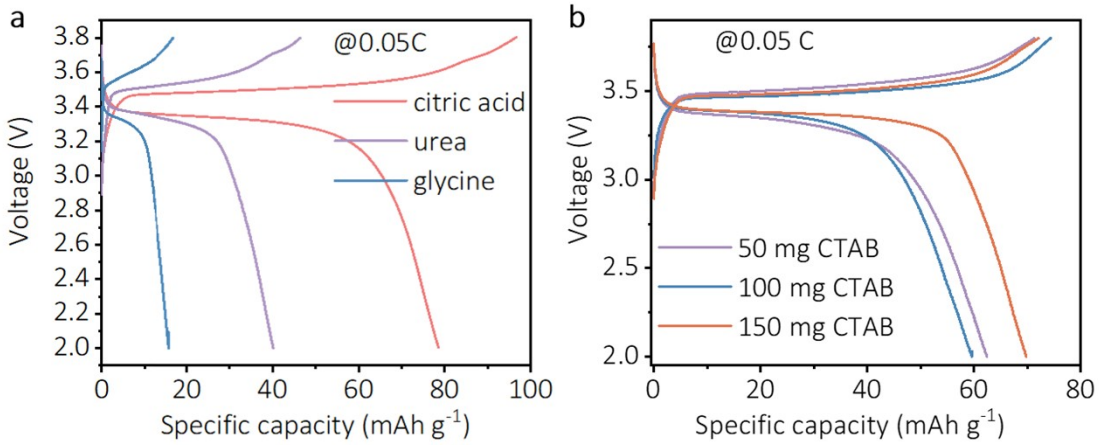

Figure S12. (a) Galvanostatic charge/discharge profiles of 3D LFP/pAlN electrode using different organic fuels (citric acid, urea and glycine) and (b) different amount of CTAB (50 mg, 100 mg, 150 mg).

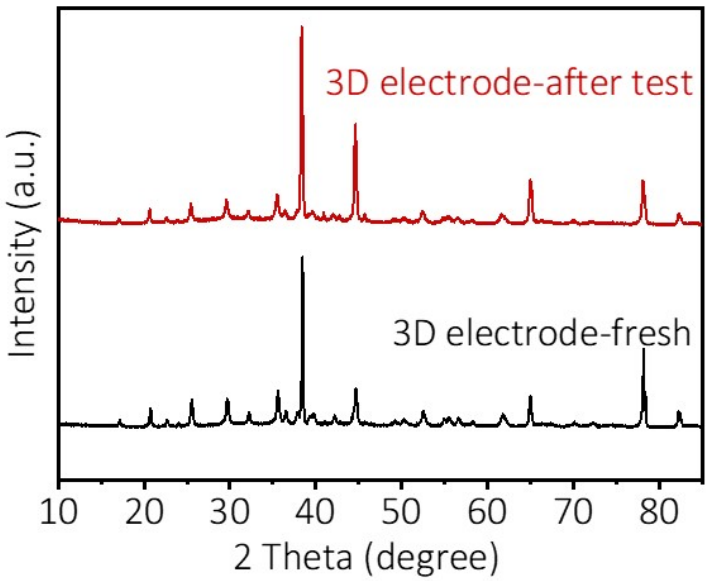

Figure S13. XRD curves of the 3D electrode powder before and after galvanostatic charge/discharge cycles.

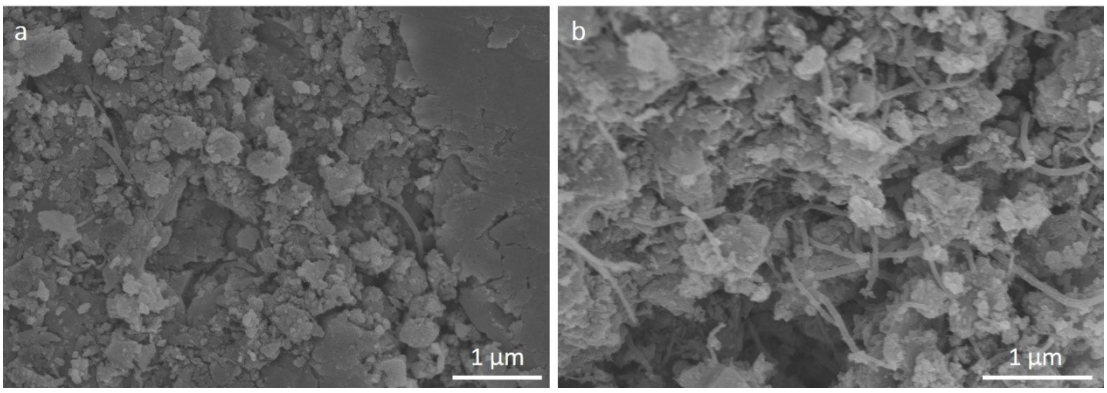

Figure S14. The SEM image of the 3D electrode after galvanostatic charge/discharge cycles.

Table S1. The calculation of porosity of Al foam.

Resistance (Ω)	m (mg)	thickness (mm)	ρ_f (g·cm^{-3})	Porosity
7.8	66.1	0.869	0.49	81.7
12	72.3	0.944	0.50	81.6
28	83.1	0.898	0.60	77.7
8	76.1	0.934	0.53	80.4
2.7	80.2	0.958	0.54	79.9
4.6	85.1	0.933	0.59	78.1
3.1	83.3	0.962	0.56	79.2
2.5	79.4	0.949	0.54	79.9
5.8	84.9	0.923	0.60	77.9
4.2	82.3	0.969	0.55	79.6
4	77.2	0.96	0.52	80.7
3.1	70.6	0.953	0.48	82.2

The porosity is calculated by:

$$Porosity = 1\_\rho_f/\rho_{Al}$$

The average porosity of Al foam is 79.9.

Table S2. The BET surface areas of pAIN and 3D LFP/pAIN electrode.

Sample	S_{BET} (m^2g^{-1})
pAlN	24.37
3D LFP/pAlN electrode	14.20

Table S3. Performance comparison of 3D LFP/pAlN electrode with recently reported novel structure 3D electrodes using non-situ growth methods.

Electrode structure	Mass loading (mg cm^{-2})	Cycles	Areal capacity (mAh cm^{-2})	Ref.
3D LFP/pAlN electrode	65	100	6.56	This work
Magnetically aligned Fe_3O_4-modified graphite flakes	9.1	50	0.93	1
$LiFePO_4$ slurry in wood-templating	60 ($LiFePO_4$)	140	3.8	2
Copolymer-aligned structure of NMC811 secondary particle	50	50	8.84	3
$LiFe_{0.7}Mn_{0.3}PO_4$ nanoplates on 3D graphene frameworks with aligned vertical channels	21.2	500	1.77	4
Electrophoretic deposition of $LiFePO_4$ onto 3D carbon fiber cloth	20 ($LiFePO_4$)	100	2	5
Micrometer-size bulk-porous Si/carbonized polyacrylonitrile composites	1.6	50	3	6
Thick porous $LiFePO_4$/C composite electrodes by spark plasma sintering	≈150	20	21	7
Freestanding $Li_4Ti_5O_{12}$/Super P/PVDF electrode	14	100	1.95	8

Table S4. Performance comparison of 3D LFP/pAlN electrode with recently reported porous and conductive 3D electrodes using in situ grown methods.

Electrode structure	Mass loading ($mg \cdot cm^{-2}$)	Cycles	Areal capacity ($mAh \cdot cm^{-2}$)	Ref.
3D LFP/pAlN electrode	**65**	**100**	**6.56**	**This work**
3-D nanoporous network composed of NiCuMn@oxide core@shell structures supported by an intercalary Cu film	6.9 (NiCuMn oxide)	100	6.1	9
FeOx porous nanoblocks array on Cu foam	2.5 (FeOx)	50	3.33	10
Outer few-layer NiO nanoflowers@medial NiO layer@Ni foam	-	100	1.45	11
Thick mesoporous Co_3O_4 nanosheet on Ni foam	4.15 (Co_3O_4)	30	4.39	12
Carbon-encapsulated Fe_3O_4 nanospheres anchored on CNT network	0.8	500	0.32	13
$LiMn_2O_4$@C grown on CNT	2	1000	0.11	14
$LiMn_2O_4$@C grown on carbon nanofiber	2	1000	0.18	14
Carbon fiber cloth coated with exfoliated porous N-doped carbon fiber, NiO nanosheets, and carbon quantum dots	10.58	250	2.91	15
MoS_2 nanoflakes grown on the twine carbon fibers of the carbonized cotton cloth	4.4 (MoS_2)	35	5.2	16
Nb_2O_5@3D holey-graphene framework composites	6	10000	1	17

References

1. Billaud J, Bouville F, Magrini T, Villevieille C, Studart AR. Magnetically aligned graphite electrodes for high-rate performance Li-ion batteries. *Nat. Energy* **1**, 16097 (2016).

2. Chen C*, et al.* Highly Conductive, lightweight, low-Tortuosity carbon frameworks as ultrathick 3D current collectors. *Adv. Energy Mater.* **7**, 1700595 (2017).

3. Yang K*, et al.* Constructing a highly efficient aligned conductive network to facilitate depolarized high-areal-capacity electrodes in Li-ion batteries. *Adv. Energy Mater.* **11**, 2100601 (2021).

4. Zhao Z*, et al.* Sandwich, vertical-channeled thick electrodes with high rate and cycle performance. *Adv. Funct. Mater.* **29**, 1809196 (2019).

5. Moyer K, Carter R, Hanken T, Douglas A, Oakes L, Pint CL. Electrophoretic deposition of $LiFePO_4$ onto 3-D current collectors for high areal loading battery cathodes. *Mater. Sci. Eng. B* **241**, 42-47 (2019).

6. Han X*, et al.* Scalable Engineering of bulk porous Si anodes for high initial efficiency and high-areal-capacity lithium-ion batteries. *ACS Appl. Mater. Interfaces* **11**, 714-721 (2019).

7. Elango R, Demortière A, De Andrade V, Morcrette M, Seznec V. Thick binder-free electrodes for Li-ion battery fabricated using templating approach and spark plasma sintering reveals high areal capacity. *Adv. Energy Mater.* **8**, 1703031 (2018).

8. Harks P-PRML*, et al.* Immersion precipitation route towards high performance thick and flexible electrodes for Li-ion batteries. *J. Power Sources* **441**, 227200 (2019).

9. Zhang S*, et al.* Ultrahigh areal capacity of self-combusted nanoporous NiCuMn/Cu flexible anode for Li-ion battery. *Chem. Eng. J.* **383**, 123097 (2020).

10. Zhang F*, et al.* 3D copper foam@FeO_x nanoarrays as a high areal capacity and stable electrode for lithium-ion batteries. *ACS Appl. Energy Mater.* **1**, 5417-5427 (2018).

11. Li Y-F*, et al.* Carbon/binder-free NiO@NiO/NF with in situ formed interlayer for high-areal-capacity lithium storage. *Adv. Energy Mater.* **9**, 1803690 (2019).

12. Wang X*, et al.* High areal capacity Li ion battery anode based on thick mesoporous

Co_3O_4 nanosheet networks. *Nano Energy* **5**, 91-96 (2014).

13. Zhou S*, et al.* Sub-thick electrodes with enhanced transport kinetics via in situ epitaxial heterogeneous interfaces for high areal-capacity lithium ion batteries. *Small* **17**, 2100778 (2021).

14. Yu X*, et al.* A dual-carbon-anchoring strategy to fabricate flexible $LiMn_2O_4$ cathode for advanced lithium-ion batteries with high areal capacity. *Nano Energy* **67**, 104256 (2020).

15. Huang Y*, et al.* Adsorption energy engineering of nickel oxide hybrid nanosheets for high areal capacity flexible lithium-ion batteries. *Energy Storage Mater.* **25**, 41-51 (2020).

16. Shan X, Zhang S, Zhang N, Chen Y, Gao H, Zhang X. Synthesis and characterization of three-dimensional MoS_2@carbon fibers hierarchical architecture with high capacity and high mass loading for Li-ion batteries. *J. Colloid Interface Sci.* **510**, 327-333 (2018).

17. Sun H*, et al.* Three-dimensional holey-graphene/niobia composite architectures for ultrahigh-rate energy storage. *Science* **356**, 599-604 (2017).